Published in final edited form as:
Biomaterials. 2010 February ; 31(4): 779–791. doi:10.1016/j.biomaterials.2009.09.082.

Long-Term Biostability of Self-Assembling Protein Polymers in the Absence of Covalent Crosslinking

Rory E. Sallach[1,5,†], **Wanxing Cui**[1,†], **Fanor Balderrama**[1,5], **Adam W. Martinez**[1,5], **Jing Wen**[1], **Carolyn A. Haller**[1], **Jeannette V. Taylor**[4], **Elizabeth R. Wright**[2,4], **Robert C. Long Jr.**[3], and **Elliot L. Chaikof**[1,5,6,*]

[1] Department of Surgery, Emory University, Atlanta, GA 30332

[2] Department of Pediatrics, Emory University, Atlanta, GA 30332

[3] Department of Radiology, Emory University, Atlanta, GA 30332

[4] Robert P. Apkarian Integrated Electron Microscopy Core, Emory University, Atlanta, GA 30332

[5] Department of Biomedical Engineering, Emory University/Georgia Institute of Technology, Atlanta, GA 30322

[6] School of Chemical and Biomolecular Engineering, Georgia Institute of Technology, Atlanta, GA 30322

Abstract

Unless chemically crosslinked, matrix proteins, such as collagen or silk, display a limited lifetime *in vivo* with significant degradation observed over a period of weeks. Likewise, amphiphilic peptides, lipopeptides, or glycolipids that self-assemble through hydrophobic interactions to form thin films, fiber networks, or vesicles do not demonstrate *in vivo* biostability beyond a few days. We report herein that a self-assembling, recombinant elastin-mimetic triblock copolymer elicited minimal inflammatory response and displayed robust *in vivo* stability for periods exceeding 1 year, in the absence of either chemical or ionic crosslinking. Specifically, neither a significant inflammatory response nor calcification was observed upon implantation of test materials into the peritoneal cavity or subcutaneous space of a mouse model. Moreover, serial quantitative magnetic resonance imaging, evaluation of pre- and post-explant ultrastructure by cryo-high resolution scanning electron microscopy, and an examination of implant mechanical responses revealed substantial preservation of form, material architecture, and biomechanical properties, providing convincing evidence of a non-chemically or ionically crosslinked protein polymer system that exhibits long-term stability in vivo.

Keywords

Recombinant protein polymer; elastin-mimetic; biocompatibility; biostability; magnetic resonance imaging

*Address correspondence to: Elliot L. Chaikof, M.D., Ph.D., 101 Woodruff Circle, Room 5105, Emory University, Atlanta, GA 30322, Tel: (404) 727-8413, Fax: (404) 727-3660, echaiko@emory.edu.
†RES and WC contributed equally to this manuscript

1. INTRODUCTION

Elastin-based protein polymers, genetically engineered with or without cell binding motifs, crosslinking domains, or non-natural amino acids, represent a promising new class of biomaterial. Their capacity to be processed as gels [1–3], films [4,5], or nanofibers [6,7] demonstrate the versatility of these recombinant proteins with potential applications in drug delivery [1,8,9], tissue engineering [10,11] or as constituents of implanted medical devices [12,13]. The majority of these proteins have been examined as covalently crosslinked networks [6,14–22].

Recently, we have reported the synthesis of amphiphilic elastin-mimetic protein polymers composed of complex block sequences that self-assemble through the formation of robust physical crosslinks [3,4,7,23]. The biosynthetic scheme for generating self-assembling recombinant proteins has been based upon a convergent strategy for integrating multiple blocks of concatemerized DNA cassettes by sequential ligation [1,7,20]. To date, this strategy has been used to design diblock, triblock, and tetrablock copolymers ranging from 100 to 200 kDa in molecular weight [3–5,7,12,23,24]. The segregation of protein blocks into compositionally, structurally, and spatially distinct domains affords ordered structures on the nanometer to micrometer size range. Significantly, protein polymers that are structurally polymorphic display tunable mechanical, chemical, and biological properties [3,4,7,23].

We have recently synthesized a triblock copolymer, designated **B9**, that contains identical hydrophobic endblocks with $[(IPAVG)_4(VPAVG)]$ repeat sequences, separated by a central hydrophilic block with repeating units of $[(VPGVG)_2(VPGEG)(VPGVG)_2]$ [1]. Phase behavior and mechanical properties of elastin-mimetic polypeptides are critically dependent on the identity of the residues within the pentapeptide repeat unit Val/Ile-Pro-Xaa-Yaa-Gly. Yaa modulates the coacervation or inverse transition temperature (T_t) in water in a manner commensurate with the polarity of the amino acid side chain and polymer-solvent interactions. Substitution of Ala for Gly in the third position of the repeat results in a change in mechanical response from elastic to plastic [25]. Thus, the midblock of **B9** displays elastic-like behavior with spectroscopic features consistent with structural conformations of native elastin, including a highly mobile backbone, β-turns, and a loose helical β-spiral. The presence of glutamic acid in the midblock raises the inverse transition temperature, preventing coacervation of the midblock over a temperature range exceeding 75°C. Nonetheless, these protein polymers reversibly self-assemble from concentrated aqueous solution above the T_t of the hydrophobic endblocks (~18°C) to form a stable, water solvated, interlocking network. Two-dimensional Fourier transform infrared (FTIR) spectroscopy reveals that above the T_t, endblock secondary structure changes from helix to sheet with the assembly of physical crosslinks [24]. Due to the presence of Ala in the third position of the pentapeptide repeat, the hydrophobic endblocks form relatively rigid domains that display plastic-like behavior. Prior investigations from our group have confirmed robust viscoelastic and mechanical responses for this, as well as for other related elastin-mimetic triblock copolymers [3–5,7].

In vivo studies have demonstrated excellent blood contacting properties in a primate arteriovenous shunt model when the triblock copolymer, **B9**, is coated as a thin film on the lumen of a small diameter vascular graft [12]. However, long-term biocompatibility and biostability for any of the members of this new class of physically crosslinked protein-based material has yet to be fully defined. Indeed, it is possible that amphiphilic protein hydrogels would display significant *in vivo* instability, given the existence of naturally occurring amphiphiles in biological fluids, such as phospholipids, glycolipids, and lipoproteins. Such amphiphiles could act as surfactants destabilizing the virtual crosslinks of protein-based material whose structural integrity is based on the association of hydrophobic domains. While structural instability may be acceptable for biodegradable systems, it has the potential to

severely limit the longevity of biomaterials whose integrity is related to hydrophobic interactions. Many *non-covalently* crosslinked self-assembled systems, such as amphiphilic peptides, lipopeptides, or glycolipids that form thin films or fiber networks are useful for drug delivery where the half-life of the system is on the order of hours. In general, none of these approaches demonstrate stability beyond a few days [26–28].

We report herein that a virtually crosslinked elastin-mimetic triblock copolymer exhibits long-term biostability and exceptional biocompatibility over a period exceeding 1 year. In conducting these studies, we have employed serial quantitative magnetic resonance imaging, evaluation of pre- and post-explant ultrastructure by cryo-high resolution scanning electron microscopy, and an examination of implant mechanical responses to characterize changes in form, material architecture, and biomechanical properties. All told, these studies reveal a non-chemically or ionically crosslinked protein polymer system that exhibits long-term stability in vivo.

2. MATERIALS and METHODS

2.1 Synthesis and purification of the elastin-mimetic triblock copolymer B9

The recombinant protein polymer **B9** was derived from concatemerization of elastin-mimetic peptide sequences, as previously described [1]. The structure consists of an ABA triblock where:

A block:	$VPAVG[(IPAVG)_4(VPAVG)]_{16}IPAVG$
B block:	$VPGVG[(VPGVG)_2VPGEG(VPGVG)_2]_{48}VPGVG.$

Individual colonies of **B9** in pET24-a in *E. coli* strain BL21 (DE3) were used to inoculate 30 mL of Circle Grow liquid media (Q-BIOgene) supplemented with the antibiotic kanamycin (50 μg/mL) and grown overnight at 37°C with shaking. A total of 5% vol/vol of the overnight culture was used to inoculate large expression flasks containing 500 mL of Circle Grow media and antibiotic, followed by a 24 hour expression at 37°C with shaking.

Cells were harvested through centrifugation in sterile tubes at 1660 RCF for 20 minutes at 4° C. The supernatant was carefully decanted, cell pellets were resuspended in cold, sterile phosphate buffered saline (PBS; 20 mL per large culture flask pellet) and frozen at −80°C. Three freeze (−80°C)/thaw (25°C) cycles were employed for the initial cell fracture with equilibration back to cold temperatures following the cycles. Once cells were completely resuspended, six cycles of sonication, consisting of 20 second pulses with 20 seconds between each pulse in an ice bath, was employed to thoroughly break the cells. To recover any unbroken cells, a preparative centrifugation step was used at 1660 RCF for 10 minutes at 4°C. Unbroken cells, which pelleted out during the spin, were resuspended in cold, sterile PBS and re-sonicated, as described above.

The cold cell lysate was centrifuged at 20,000 g for 40 minutes at 4°C. The supernatant was transferred to a cold, sterile tube and poly(ethyleneimine) (PEI) was added to a final concentration of 0.5%. This solution was centrifuged again at 20,000g for 40 minutes at 4°C to remove all nucleic acids and contaminating cellular material precipitated by the PEI. The supernatant was transferred to 50 mL Falcon tubes and NaCl was added to a final concentration of 2M. The elastin-mimetic protein was salted out of solution at 25°C for 30–45 minutes. This solution was centrifuged at 9500 g for 15 minutes at 25°C to recover the protein product (‘hot-spin’). The supernatant was discarded and the protein pellet was resuspended in cold, sterile PBS on ice for up to 10–20 minutes to avoid solubilizing unwanted contaminates. The resuspended solution was then subjected to a ‘cold spin’ at 20,000 g for 40 minutes at 4°C. The supernatant was transferred to sterile 50 mL tubes and salting precipitation repeated. The

hot (25°C)/cold (4°C) spin cycles were repeated until a contaminating pellet was no longer observed after the cold spin. Typically, 6–10 cycles were required followed by a hot spin.

For *in vivo* studies, **B9** underwent a secondary treatment with sodium hydroxide. The protein pellet was resuspended in cold, sterile PBS at approximately 50 mg per 20 mL. Sterile sodium hydroxide was added to a final concentration of 0.4 N and mixed gently by hand. The mixture was incubated on ice for fifteen minutes, after which 5M sodium chloride was added to a final concentration of 2M. The protein was precipitated from solution at 25°C, centrifuged at 8500 g for 20 minutes at 25°C, and resuspended in cold PBS. This treatment was repeated three times. Following the third treatment, the protein solution was adjusted to pH 6–8. A cold spin was performed at 20,000 rpm for 40 minutes at 4°C and the supernatant was desalted using a PD-10 desalting column (GE Healthcare Lifesciences) with molecular grade water (Cellgro). The end product was passed through 0.2 μm filter, eluted into autoclaved Lyoguard freeze drying trays (Gore), frozen at −80°C, and lyophilized. This procedure afforded **B9** as a white fibrous protein product with isolated yields of 50 mg/L of expression culture.

Lyophilized **B9** was resuspended in sterile molecular grade water at 1 mg/mL and endotoxin levels were assessed using the Limulus Amoebocyte Lysate (LAL) assay (Cambrex). Levels of endotoxin were typically 0.1 EU/mg of protein polymer (1 EU = 100 pg of endotoxin).

2.2 Structural characterization of the elastin-mimetic triblock copolymer B9

2.2.1 Gel electrophoresis—Protein size and purity was assessed by sodium dodecyl sulfate-polyacrylamide gel electrophoresis (SDS-PAGE). A total of 10 μg of the elastin-mimetic polypeptide was run on a 7.5% gel along with Precision Plus Protein Kaleidoscope (Bio-Rad) molecular weight markers and negatively stained with Copper (Bio-Rad). MALDI-TOF mass spectrometry identified a 165 kDa protein and the sequence was confirmed by amino acid compositional analysis [3].

2.2.2 Evaluation of water content in protein gels—For evaluation of water content, 200 μL of a 10-wt% protein solution was cast as a disk measuring 1 cm in diameter. Samples were first dried at room temperature under controlled water evaporation conditions and then fully dehydrated under vacuum. Specimens were subsequently incubated in PBS at 37 °C for 24 h and fully hydrated weights were obtained. The equilibrium water content and equilibrium swelling ratio were determined according to Eqs. (1) and (2), respectively, and expressed as mean ± standard deviation.

$$\text{Equilibrium water content} = [(\text{hydrated weight} - \text{dehydrate weight})]/(\text{hydrated weight}) \quad (1)$$

$$\text{Equilibrium swelling ratio} = (\text{hydrated weight})/(\text{dehydrated weight}) \quad (2)$$

2.2.3 Rheological analysis of concentrated B9 solutions—Rheological data were acquired on an Advanced Rheological Expansion System III rheometer (ARES III, TA instrument, NJ) in parallel plate geometry with a plate diameter of 25 mm. The testing protocol for rheological analysis has been detailed elsewhere [7]. In brief, protein solutions were prepared at 100 mg/mL by adding distilled, deionized water to lyophilized protein at 4°C, shaking the solution for 48 hours, and then allowing the solution to equilibrate for 72 hours. The gap between parallel plates was adjusted between 0.2 – 0.35 mm and dynamic mechanical experiments were performed in shear deformation mode. The gelation temperature was

determined by heating samples from 4°C to 37°C at a rate of 1°C per minute. Experiments were repeated on three samples and representative data presented.

2.3 Short-term implant studies

2.3.1 Subcutaneous injection—According to a protocol approved by Emory University Institutional Animal Care and Use Committee (IACUC), **B9** protein solutions were injected into the subcutaneous space of 8 week old inbred male C57BL/6 mice weighing 25–30 g obtained from Jackson Laboratory (Bar Harbor, ME). Mice were sedated using ketamine (95 mg/kg, IM) and xylazine (5 mg/kg, IM). A total of 200 μL of 100 mg/mL solution of endotoxin free **B9** was injected into the interstitial fascia where it immediately gelled. A set of three mice each received a single injection. All injections were conducted in the cold room using chilled syringes, needles, and solutions. Mice were immediately warmed following the injection. Three weeks after implantation, mice were sacrificed and the hydrogel explanted along with overlying skin.

2.3.2 Peritoneal cavity injection—According to a protocol approved by Emory University Institutional Animal Care and Use Committee (IACUC), **B9** protein solutions were injected into the peritoneal cavity of 8 week-old inbred male C57BL/6 mice weighing 25–30 g obtained from Jackson Laboratory (Bar Harbor, ME). Mice were sedated using ketamine (95 mg/kg, IM) and xylazine (5 mg/kg, IM) prior to protein injections. A total of 200 μL of 100 mg/mL solution of endotoxin free **B9** was injected into the peritoneal cavity where it immediately gelled. A set of five mice each received a single injection. All injections were conducted in the cold room using chilled syringes, needles, and solutions. Mice were immediately warmed following the injection. One week after implantation, mice were sacrificed, and free cells in the peritoneal cavity were harvested by saline lavage for FACS analysis, as detailed below, prior to harvesting the hydrogel for histological assessment.

2.3.3 Fluorescent-activated cell sorting (FACS) analysis of peritoneal lavage—Prior to harvesting implants, each peritoneal cavity was lavaged with 10 mL of cold Hank's Balanced Salt Solution containing 10 U/mL heparin and 1% BSA (Mediatech, Inc). Typically, 6 to 7 mL of lavage solution was retrieved and cells immunostained for flow cytometry with PE-conjugated rat monoclonal anti-mouse CD11b for macrophage, FITC-conjugated hamster anti-mouse CD3 for total T cells, FITC-conjugated rat monoclonal anti-mouse CD4 for helper T cells, FITC-conjugated rat monoclonal anti-mouse CD8 for cytotoxic T cells, FITC-conjugated rat monoclonal anti-mouse CD19 for B cells, and FITC-conjugated rat monoclonal anti-mouse Gr-1 for neutrophils (BD Biosciences Pharmingen). Antibodies were diluted in staining buffer (PBS pH 7.4 containing 1% BSA and 0.1% sodium azide) to 1 μg/50 μL/10^6 cells, incubated with cells for 30 minutes in the dark on ice, washed three times in staining buffer, and fixed in 1% paraformaldehyde. Analysis was performed on a FACScan using Cellquest (Becton Dickinson) and FlowJo software (Tree Star).

2.3.4 Histological examination—Retrieved hydrogel samples were processed for histological and immunohistochemical evaluation to facilitate identification of cell types present. All samples were fixed overnight in 10% neutral buffered formalin and processed for paraffin embedding. Sections were prepared at a thickness of 5 μm and stained with hematoxylin and eosin (H&E) or rat anti-mouse monoclonal F4/80 (CI:A3-1, Abcam) for infiltrating macrophages. In all cases, multiple sections for each of three to five samples were examined. Fibrous capsule thickness was measured from optical micrographs. Values for capsule thickness represent mean ± standard deviation as determined from at least six distinct regions on each surrounding capsule in which each region is represented by a minimum of 10 high power fields.

2.4 Long-term implant studies

2.4.1 Fabrication of cylindrical protein polymer implants—A cold solution of **B9** at 100 mg/mL was drawn into a chilled 1 mL syringe (Becton Dickenson), equilibrated at 4°C for 30 minutes, and subsequently gelled at 37°C. The tip of the syringe was removed with a sterile scalpel and the molded protein gel extruded into room temperature PBS, equilibrated overnight under a bio-hood, and then sectioned into 8 mm × 4.76 mm cylindrical test samples.

2.4.2 In vivo biostability—All animal experiments were approved by the Institutional Animal Care and Use Committee (IACUC) at Emory University. Eight-week-old inbred male C57BL/6 mice weighing 25–30 g were obtained from Jackson Laboratory (Bar Harbor, ME). Under ketamine (95 mg/kg, IM) and xylazine (5 mg/kg, IM) anesthesia, a 1 cm dorsal midline incision was performed and a cylindrical gel implanted in the subcutaneous space, parallel to the spine. Eight mice were enrolled and serial MR imaging performed weekly for 6 weeks and every other week thereafter. During scanning, 2.5% isoflurane inhalation was utilized for induction followed by 1.8% isoflurane throughout the duration of imaging. Total scan time for each animal was less than one hour. At the termination of the study, all mice were sacrificed and samples with surrounding tissue harvested for immunohistochemical analysis, as detailed previously. Von Kossa staining was used to assess for the presence of calcium.

2.4.3 ^{1}H Magnetic resonance imaging—MR imaging was performed using a Varian/Inova 4.7 T horizontal bore magnet operating at 200.56 MHz (Varian, Inc). The magnet was equipped with an 11.7 cm inner diameter shelf-shielded gradient system with a maximum gradient strength of 25 gauss/cm. Constructs implanted in mice were investigated using transmit/receive 16-element quadrature birdcage coil with an inner diameter of 3.8 cm. Each anesthetized mouse was secured in a home-built cradle and the implant centered within the magnetic field.

Exact positioning of the construct was determined using several fast-spin echo scout scans. A final high resolution fast-spin echo image (relaxation time, T_R = 2.0 sec, echo spacing, esp = 14 μs at number of averages, nt = 2) was collected to provide a more detailed image of the construct structure and surrounding microenvironment. A fast-spin echo sequence with an echo train length (ETL) of 8 was utilized, which afforded a field of view of 3.5 × 3.5 cm with a slice thickness of 0.5 mm.

Characteristically, transverse images of each implant consisted of 23 slices at a thickness of 500 μm. The acquired data contained 256 × 256 points and was zero filled to 512 points in both the read and phase encoded directions. A 2-D Fourier transformation was performed, which provided a final in-plane resolution of 68 × 68 μm with a slice thickness of 500 μm. Cross-sectional area and length measurements were performed using the image processing program, Image J (NIH). Implant volumes were calculated using Simpson's method of numerical integration of cross-sectional areas.

2.4.4 Cryo high resolution scanning electron microscopy (HRSEM)—Hydrated protein polymer samples were examined either prior to implantation or at the time of implant retrieval. Samples were plunged into liquid ethane at its melting point (−183°C), stored in liquid nitrogen (LN_2), and transferred to a precooled (ca. −170°C) Oxford CT-3500 cryo-stage held in a cryo-preparation chamber. The shutters on the stage were closed to minimize frost contamination and the cryo-stage was transferred to the Denton DV-602 Cr coater. The stage was first allowed to equilibrate to −170°C in a vacuum of ~10^{-7} torr. In order to remove excess, unbound water (vitreous ice) from the samples the shutters were then opened and the stage brought to a temperature of −105°C for varying time intervals. The stage shutters were closed and the stage was returned to −170°C. In select instances, the bulk phase was examined by

fracturing specimens with a pre-chilled blade and washed with LN2. A thin (3 nm) film of chromium was sputter coated onto the specimen and the stage transferred to the upper stage of the DS-130F field-emission SEM operated at 25 kV. During the imaging process, specimen temperature was maintained at −120°C

2.4.5 Biomechanical analysis—Mechanical responses of protein polymer samples were characterized by compression testing prior to implantation and at the time of specimen removal, one year after initial implantation. Cylindrical specimens were fabricated as described above. At the time of explantation, samples were placed in PBS containing sodium azide (0.2 mg/mL) maintained at 37°C. The fibrous capsule was removed to facilitate testing and did not damage the implant upon removal. Gels were photographed and tested within 24 hours of harvest. All samples examined by optical microscopy to ensure the absence of gross defects and were cut to a thickness of 2.35 mm for mechanical testing.

Testing was performed using a Bose ELF system with a 1.1 lb load cell and a hydration chamber containing PBS at 37°C at the Georgia Institute of Technology Mechanical Testing Laboratory. Samples were preconditioned by cyclic compression ranging between 1% and 20% strain for 10 cycles. Compression stress-strain testing was performed at 0.025 mm/sec. Compression stress-relaxation testing was conducted by initially compressing the sample to a strain of 75% at 0.025 mm/sec followed by monitoring change in compression stress over time. Cotangent moduli were calculated from the compression stress-strain plots at 10% strain intervals between 20% and 60% strain. Specifically, a linear regression was performed on the points at a given % strain ± 1% strain. For example, at 10% strain, data points from 9% to 11% strain were plotted against the compression stress.

2.5. Statistical analysis

Comparison between groups was analyzed using a Student's t-test and all results presented as mean ± SEM. At least four to eight mice were enrolled in each experimental and control group for all conducted studies.

3. RESULTS

3.1 Molecular and rheological properties of protein polymer B9

Gel electrophoresis of **B9** revealed a single band at 170 kDa consistent with prior studies from our laboratory (Fig. 1A) [3,7,12]. Likewise, rheological behavior of aqueous solutions of **B9** was unchanged after NaOH treatment with an observed sol-gel transition at 18°C. The gel point of protein solutions can be detected by measurement of the shear storage (G′) and loss (G″) modulus as a function of temperature at a fixed frequency. Above 18°C, G′ and G″ increased while tan δ (G′/G″) decreased, consistent with the formation of a viscoelastic gel (Fig. 1B). The equilibrium water content and swelling ratio of a 10-wt% gel were 81.5 ± 0.51% and 5.41 ± 0.15, respectively (n = 4).

3.2 Short-term host-implant responses

To assess early *in vivo* responses to **B9** hydrogels, a 10-wt% solution of protein polymer was injected into either the subcutaneous space or the peritoneal cavity in a mouse model. Peritoneal samples were retrieved one week after implantation and subcutaneous samples explanted at three weeks (Figs. 2, 3). Retrieved samples were irregularly shaped, but optically transparent. A thin fibrous capsule surrounded all implants with an observed capsule thickness of 36 ± 6μm for subcutaneous specimens and 16 ± 3 μm for peritoneal samples without evident cellular infiltration into implants in either subcutaneous or peritoneal locations. Macrophages were noted along the periphery of the fibrous capsule consistent with a mild foreign body response. FACS analysis of peritoneal cells did not reveal significant differences between mice

undergoing sham surgery or those receiving an implant, as well as non-operated mice (data not shown) (Fig. 4).

3.3 Long-term host-implant responses

MR imaging provides a useful means for *in situ* characterization of subcutaneously implanted biomaterials. Adequate contrast was achieved between the implant and surrounding tissue, which reflected the high water content of the protein gel (Fig. 5). Implant cross sectional areas, lengths, and volumes were assessed through image analysis over a 12-month period (Fig. 6). Cross-sectional area decreased by 30% and volume by 40% over an initial 2–3 month period with relatively little change in implant dimension thereafter. Apart from a decrease in implant dimension, MR imaging did not reveal any other notable finding. At sample retrieval one year after implantation, gels were intact without evidence of an inflammatory or other cellular infiltrate (Fig. 7). Macrophages were noted at the periphery of the implant. Von Kossa staining did not reveal the presence of calcium deposits (Fig. 8). The thickness of the fibrous capsule was 80 ± 8 μm (mean ± SD; Fig. 9).

High-resolution cryo-SEM revealed that gel ultrastructure remained stable thoughout the implant period (Fig. 10). Gels displayed open cell morphology (pore diameter ca. 400–500 nm), both prior to implantation and after a 1-year implant period. No discernable differences were noted between surface and bulk ultrastructure of the protein gels. Compression testing was performed to assess gel mechanical properties. Compared to pre-implant values, after one year *in vivo* a modest reduction in the cotangent compressive modulus and an increase in the stress-relaxation response were observed (Fig. 11).

4. DISCUSSION

Molecular self-assembly is ubiquitous in nature and has recently been exploited for biomaterial design. Self-assembly is mediated by a number of weak, noncovalent bonds, including hydrogen bonding, as well as electrostatic, hydrophobic, and van der Waals interactions ultimately forming higher order structures. One such example of natural molecular self-assembly is tropoelastin, which coacervates to align tropoelastin molecules in preparation for intermolecular crosslinking. At ambient temperatures, tropoelastin is soluble in aqueous solutions, however, as the temperature is raised, molecular aggregation occurs through hydrophobic interactions. Coacervation is a lower critical solution temperature (LCST) phenomenon in which the protein forms a more ordered system upon increasing temperature. The same phenomena has been observed with recombinant elastin proteins where precise control over the temperature at which coacervation occurs has been correlated with amino acid sequence and exploited for tunable control over the assembly process [29].

Tissue-material responses, including the rate and extent of biodegradation, are integral to assessing the suitability of elastin-like biopolymers for implant related applications. To date, reports documenting *in vivo* responses to elastin-mimetic protein implants have been limited; largely confined to several studies performed 15 to 20 years ago on proteins synthesized chemically and subject to radiation crosslinking [30,31]. In these investigations, homopolymers or copolymers composed of VPGVG, VPGKG, VPGEG, IPAVG, and VPAVG reportedly did not induce significant inflammatory or allergic reactions [30–33]. The most thoroughly characterized variant, chemically synthesized poly(GVGVP), underwent in vitro toxicity and mutagenicity assays and was administered via intravenous, intraocular, intramuscular, intraperitoneal, and subcutaneous routes without toxic effect [30,31]. A fibrous capsule was noted three weeks after intramuscular implantation of a radiation crosslinked sample [30]. In a more recent report, elastin microparticles prepared from chemically synthesized poly(VPAVG) were evaluated following subcutaneous and intravitreal injections. No inflammatory response observed after 28 days. However, tractional retinal detachment was

noted [32]. The failure to detect an immune mediated reaction to these polymers is consistent with other studies that have sought to identify potentially immunogenic epitopes on native elastin. While polyclonal and monoclonal antibodies can be raised against peptides derived from the hydrolysis of native elastin, neither VPGVG nor VPAVG peptides were among the recognized sequences [34]. Moreover, VPGVG peptides were unable to competitively inhibit the binding of any of the antibodies raised against native elastin, which further supports the notion that this pentapeptide is not present among antigenic elastin epitopes [34].

Recently, genetically engineered elastin-mimetic protein polymers have been investigated *in vivo* as non-thrombogenic coatings [12,13], targeted drug delivery vehicles [35–37], and as an implantable material [38]. In the latter instance, after a 13 week implant period in the subcutaneous space, recombinant human tropoelastin 'sponges', chemically crosslinked with bis(sulfosuccinimidyl) suberate were surrounded by a fibrous capsule with a minimal to moderate inflammatory response [38]. Non-chemically crosslinked recombinant elastin-like proteins have also been administered within the intra-articular space as a 650 μM protein solution. Although the biological response was not evaluated, this study revealed a 3 hour half-life for non-aggregating VPGVG proteins and a 3 day half-life for aggregating VPG**X**G proteins, where **X** = V:G:A at a ratio of 1:7:8 [37]. As a related material, a 47 kDa recombinant silk-elastin-like protein (SELP), comprised of GAGAS silk-like [S] and GVGVP elastin-like [E] amino acid sequences ($[S]_4[E]_4[EK][E]_3$) has been studied after injection into the subcutaneous space. Histological analysis revealed minimal fibrous encapsulation after four weeks with a mild degree of inflammation that included the presence of macrophages in the surrounding tissue [39]. SELPs have also been used for adenoviral gene delivery and demonstrate prolonged and localized expression of adenoviruses for up to 15 days, suggesting the potential for cancer gene therapy [40]. A summary of *in vivo* biocompatibility studies conducted on elastin-mimetic proteins is presented in Table 1.

The evaluation of *in vivo* biocompatibility has largely been based on characterizing local tissue responses to subcutaneously implanted materials where the intensity and duration of the inflammation and wound healing, including capsule formation, is evaluated histologically. Although histological studies of biopolymers containing elastin-mimetic sequences have previously noted the presence of 'mild inflammation' [31,32] and 'a reaction that was limited to a typical cell mediated response to the presence of a foreign body' [38], the extent of fibrous capsule thickness has not been reported. Fibrous capsule thickness has been investigated for a variety of polymeric and ceramic implants designed for tissue repair, cell encapsulation, or as drug delivery systems [41–45]. Capsule thicknesses are dependent on implant site and material type and typically vary between 2 and 150 μm over implantation periods of one to three months. For example, greater capsule thickness has been observed for materials within intraperitoneal sites compared to those in subcutaneous sites over identical implant durations [42]. Ceramic materials, aluminum calcium phosphate, hydroxyapatite, and tricalcium phosphate, appeared to invoke the mildest inflammatory response with the thinnest fibrous capsule, approximately 2.5 μm and 6 μm, after 90 day implant periods in the subcutaneous and peritoneal cavities, respectively [42]. As an illustration of the effects of surface chemistry, implants comprised of poly(alkyl methacrylate) (PAMA) with short alkyl side chains exhibited a thicker fibrous capsule than those with long side chains (140 μm vs 120 μm) [41]. Additionally, self-assembled monolayers of alkanethiols on gold with different terminal functional groups displayed surface dependent inflammatory responses after one week in subcutaneous tissue. Hydrophobic methyl terminated surfaces induced thick fibrous capsules (130 μm) and greater recruitment of inflammatory cells, as compared to hydrophilic COOH- (80 μm) and OH- (70 μm) terminated surfaces [46]. Likewise, polypropylene implants whose surfaces were modified with –OH groups triggered formation of a thicker capsule (~100 μm) than when modified with –COOH moieties (37 μm) [47]. In contrast, surface topography does not appear to have a significant effect on capsule thickness, although it may influence local inflammatory responses [48].

Relatively inert synthetic polymers, such as, silicone, and organic biopolymers, such as cellulose also elicit a foreign body reaction after subcutaneous implantation with an observed fibrous capsule thickness of approximately 90 μm and 80 μm, respectively, at four weeks [45].

In this report, FACS analysis of peritoneal lavage fluid harvested one week after injection of **B9** demonstrated no apparent difference in either the number or type of inflammatory cells when compared to those mice not exposed to the polymer gel. Significantly, as a subcutaneous implant, the elastin-mimetic protein polymer gel initiated only a limited local inflammatory response. Moreover, the resultant fibrous capsule is among the thinnest observed to date for non-ceramic implants in comparable murine implant sites and over similar periods of implantation. This effect may be related to the presence of glutamic acid residues in the hydrophilic midblock that segregate to the surface with an enriched concentration of –COOH groups at the material-tissue interface.

Elastin-mimetic proteins such as **B9** and other multiblock systems afford the ability to form physical or virtual crosslinked networks through the self-association of chemically similar domains. In the case of elastin-mimetic proteins [1–4,7,24], repeat peptide sequences of self-associating blocks are chosen, such that coacervation or phase separation of these domains occurs in water under physiologically relevant conditions (pH 7.4, 37°C), which maximizes hydrophobic interactions that drive self-assembly. In turn, the sequence of the non-crosslinking domain is selected in a manner that precludes coacervation. This typically has required the incorporation of hydrophilic residues in the fourth position of the pentapeptide repeat sequence (Val-Pro-Gly-Xaa-Gly), such as glutamic acid, which limits the tendency for block aggregation. Physically crosslinked protein-based materials possess a number of advantages over their chemically crosslinked counterparts, including ease of processability, the ability to avoid the addition or removal of reagents or unreacted intermediates needed for chemical crosslinking, and the capacity to incorporate biologically or chemically active agents or cells that might otherwise be sensitive to covalent crosslinking schemes. Moreover, if blocks are of sufficient size and chemical diversity the potential to access diverse polymer morphologies exists. This provides the capacity to tune a wide range of functional responses, such as mechanical behavior, permeability or drug elution characteristics, as well as the potential to design templated materials.

Most biomaterials whose integrity is based on self-association of hydrophobic constituents display short-lived stability *in vivo* and have been utilized for drug delivery or wound healing applications. The instability of these systems can be attributed to natural surfactants, other amphiphilic molecules, or enzymes that promote lysis and solubulize specific lipids and proteins. Phospholipids, lipopeptides, and glycolipids have been extensively employed as drug carriers when formulated as vesicles, liposomes, or micelles, all of which have relatively short half-lives even when directly injected within tissues. Similarly, amphiphilic graft copolymers, such as alkylated carrageenan [49], poly(2-hydroxyethyl methacrylate)-g-oligolactide, or poly (ethylene glycol)-g-poly(DL-lactic acid-*co*-glycolic acid) all degrade rapidly [50]. Recently, amphiphilic peptides that self-assemble as fibrous networks have been described as vehicles for cell and drug delivery [27]. These systems display relatively rapid dissociative responses, as well. In contrast, structures that self-associate through electrostatic interactions, including calcium or barium crosslinked alginate gels or alginate-polylysine thin films, generally exhibit greater biostability [51].

A number of materials that self-assemble also require additional crosslinking for biomedical applications. Collagen has been used as a scaffold for tendon, cartilage, and bone regeneration, as well as for drug delivery, and skin substitutes. However, most collagen systems are crosslinked by a variety of chemical [52,53] or physical [54] means. In fact, non-crosslinked

collagen displays a limited lifetime *in vivo*, with significant degradation observed within three to four weeks [38,55]. Natural silk is also degradable, but over longer durations with a >50% loss of strength at 6–12 weeks [56,57]. Likewise, recombinant tropoelastin has been fabricated into a chemically crosslinked 'sponge.' Degradation was evident 13 weeks after implantation when formulated with an open porous surface enabling cells to penetrate the implant, but limited when produced with a smooth surface [38]. Similarly, crosslinking and chemical modification have been employed to reduce degradation rates of hyaluronic acid hydrogels [58].

MRI has been previously used to monitor biomaterial degradation and swelling behavior of a number of polymeric materials, including hydrogels [59,60]. In this report, MR imaging demonstrated substantial long-term durability of a self-assembled elastin-mimetic protein polymer hydrogel, even in the absence of covalent or ionic crosslinks. Furthermore, cryo-SEM confirmed preservation of biopolymer micro- and nanoscale architecture. Nonetheless, a modest reduction in compressive modulus was observed along with an increase in the stress-relaxation response, which suggests some reduction in the elastomeric nature of the material. In the absence of an obvious change in gel microstructure, these changes imply an alteration in the nature or extent of the physical crosslinks that may reflect a decrease in protein polymer mass, some disruption of hydrophobic microdomains that serve as crosslinking sites or both.

5. CONCLUSIONS

Elastin-based protein polymers are a promising class of material characterized by high degree of biocompatibility and a tunable range of mechanical properties from plastic to elastic. A variety of options facilitate the processing of these biopolymers into gels, films, or nanofibers for any of a number of implant applications in orthopedics, as well as in plastics, cardiovascular, and general surgery. Additionally, the potential exists for incorporating bioactive compounds onto the polymer backbone or within the protein matrix. Likewise, such materials provide a prospective vehicle for cell delivery. In this report we have characterized local tissue response and long-term *in vivo* biostability of a physically crosslinked recombinant elastin-mimetic copolymer. We predict elastin-mimetic triblock copolymers will find utility as structural components of artificial organs and engineered living tissues, as carriers for controlled drug release, or as biocompatible surface coatings.

Acknowledgments

This work was supported by NIH grants HL60464 and HL083867 (E.L.C.). RES and AWM were supported through NSF graduate fellowships and FB was supported through an AHA predoctoral fellowship. This research project was supported in part by the Robert P. Apkarian Integrated Electron Microscopy Core of Emory University.

References

1. Wright ER, Conticello VP. Self-assembly of block copolymers derived from elastin-mimetic polypeptide sequences. Adv Drug Deliv Rev 2002;54:1057–1073. [PubMed: 12384307]
2. Wright ER, McMillan RA, Cooper A, Apkarian RP, Conticello VP. Thermoplastic elastomer hydrogels via self-assembly of an elastin-mimetic triblock polypeptide. Advanced Functional Materials 2002;12 (2):1–6.
3. Nagapudi K, Brinkman WT, Thomas BS, Wright ER, Conticello VP, Chaikof EL. Protein-based thermoplastic elastomers. Macromolecules 2005;38:345–354.
4. Wu X, Sallach R, Haller CA, Caves JA, Nagapudi K, Conticello VP, et al. Alterations in physical cross-linking modulate mechanical properties of two-phase protein polymer networks. Biomacromolecules 2005;6(6):3037–3044. [PubMed: 16283724]

5. Wu X, Sallach RE, Caves JM, Conticello VP, Chaikof EL. Deformation responses of a physically cross-linked high molecular weight elastin-like protein polymer. Biomacromolecules 2008;9:1787–1794. [PubMed: 18558738]
6. Nagapudi K, Huang L, McMillan RA, Brinkman W, Conticello VP, Chaikof EL. Photomediated solid-state crosslinking of an elastin-mimetic recombinant protein polymer. Macromolecules 2002;35:1730–1737.
7. Nagapudi K, Brinkman WT, Thomas BS, Park JO, Srinivasarao M, Wright E, et al. Viscoelastic and mechanical behavior of recombinant protein elastomers. Biomaterials 2005;26(23):4695–4706. [PubMed: 15763249]
8. Herrero-Vanrell R, Rincon AC, Alonso M, Reboto V, Molina-Martinez IT, Rodriguez-Cabello JC. Self-assembled particles of an elastin-like polymer as vehicles for controlled drug release. J Control Release 2005;102(1):113–122. [PubMed: 15653138]
9. Dreher MR, Raucher D, Balu N, Michael Colvin O, Ludeman SM, Chilkoti A. Evaluation of an elastin-like polypeptide-doxorubicin conjugate for cancer therapy. J Control Release 2003;91(1–2):31–43. [PubMed: 12932635]
10. Liu JC, Heilshorn SC, Tirrell DA. Comparative cell response to artificial extracellular matrix proteins containing the RGD and CS5 cell-binding domains. Biomacromolecules 2004;5(2):497–504. [PubMed: 15003012]
11. Richman GP, Tirrell DA, Asthagiri AR. Quantitatively distinct requirements for signaling-competent cell spreading on engineered versus natural adhesion ligands. J Control Release 2005;101(1–3):3–12. [PubMed: 15588889]
12. Jordan SW, Haller CA, Sallach RE, Apkarian RP, Hanson SR, Chaikof EL. The effect of a recombinant elastin-mimetic coating of an ePTFE prosthesis on acute thrombogenicity in a baboon arteriovenous shunt. Biomaterials 2007;28(6):1191–1197. [PubMed: 17087991]
13. Woodhouse KA, Klement P, Chen V, Gorbet MB, Keeley FW, Stahl R, et al. Investigation of recombinant human elastin polypeptides as non-thrombogenic coatings. Biomaterials 2004;25(19):4543–4553. [PubMed: 15120499]
14. Lim DW, Nettles DL, Setton LA, Chilkoti A. Rapid cross-linking of elastin-like polypeptides with (hydroxymethyl) phosphines in aqueous solution. Biomacromolecules 2007;8(5):1463–1470. [PubMed: 17411091]
15. Bellingham CM, Lillie MA, Gosline JM, Wright GM, Starcher BC, Bailey AJ, et al. Recombinant human elastin polypeptides self-assemble into biomaterials with elastin-like properties. Biopolymers 2003;70(4):445–455. [PubMed: 14648756]
16. Lee J, Macoscko CW, Urry DW. Elastomeric polypentapeptides cross-linked into matrixes and fibers. Biomacromolecules 2001;2:170–179. [PubMed: 11749169]
17. Nowatzki PJ, Tirrell DA. Physcial properties of artificial extracellular matrix protein films prepared by isocyanate crosslinking. Biomaterials 2004;25:1261–1267. [PubMed: 14643600]
18. Trabbic-Carlson K, Setton LA, Chilkoti A. Swelling and mechanical behaviors of chemically cross-linked hydrogels of elastin-like polypeptides. Biomacromolecules 2003;4:572–580. [PubMed: 12741772]
19. McMillan RA, Conticello VP. Synthesis and characterization of elastin-mimetic protein gels derived from a well-defined polypeptide precursor. Macromolecules 2000;33:4809–4821.
20. McMillan RA, Lee TAT, Conticello VP. Rapid assembly of synthetic genes encoding protein polymers. Macromolecules 1999;32:3643–3648.
21. Zio KD, Tirrell DA. Mechanical properties of artificial protein matrices engineered for control of cell and tissue behavior. Macromolecules 2003;36:1553–1558.
22. Lim DW, Nettles DL, Setton LA, Chilkoti A. In situ cross-linking of elastin-like polypeptide block copolymers for tissue repair. Biomacromolecules 2008;9(1):222–230. [PubMed: 18163573]
23. Sun XL, Haller CA, Wu X, Conticello VP, Chaikof EL. One-pot glyco-affinity precipitation purification for enhanced proteomics: The flexible alignment of solution-phase capture/release and solid-phase separation. J Proteome Res 2005;4(6):2355–2359. [PubMed: 16335985]
24. Sallach RE, Wei M, Biswas N, Conticello VP, Lecommandoux S, Dluhy RA, et al. Micelle density regulated by a reversible switch of protein secondary structure. J Am Chem Soc 2006;128(36):12014–12019. [PubMed: 16953644]

25. Urry, D.; Pattanaik, A.; Accavitti, MA.; Luan, CX.; McPherson, DT.; Xu, J., et al., editors. Handbook of Biodegradable Polymers. Harwood: Amsterdam; 1997.
26. Rajangam K, Behanna HA, Hui MJ, Han X, Hulvat JF, Lomasney JW, et al. Heparin binding nanostructures to promote growth of blood vessels. Nano Lett 2006;6(9):2086–2090. [PubMed: 16968030]
27. Kisiday J, Jin M, Kurz B, Hung H, Semino C, Zhang S, et al. Self-assembling peptide hydrogel fosters chondrocyte extracellular matrix production and cell division: implications for cartilage tissue repair. Proc Natl Acad Sci U S A 2002;99(15):9996–10001. [PubMed: 12119393]
28. Sargeant TD, Guler MO, Oppenheimer SM, Mata A, Satcher RL, Dunand DC, et al. Hybrid bone implants: Self-assembly of peptide amphiphile nanofibers within porous titanium. Biomaterials 2008;29(2):161–171. [PubMed: 17936353]
29. Urry DW, Luan CH, Parker TM, Gowda DC, Prasad KU, Reid MC, et al. Temperature of polypeptide inverse temperature transition depends on mean residue hydrophobicity. J Am Chem Soc 1991;113:4346–4348.
30. Wood SA, Lemons JE, Prasad KU, Urry DW. In vitro calcification and in vivo biocompatibility of the crosslinked polypentapeptide of elastin. J Biomed Mater Res 1986;20(3):315–335. [PubMed: 3957967]
31. Urry DW, Parker TM. Biocompatibility of the bioelastic materials, poly(GVGVP) and its gamma-irradiation cross-linked matrix: Summary of generic biological test results. J Bioactive Compatible Polym 1991;6:263–282.
32. Rincon AC, Molina-Martinez IT, de Las Heras B, Alonso M, Bailez C, Rodriguez-Cabello JC, et al. Biocompatibility of elastin-like polymer poly(VPAVG) microparticles: In vitro and in vivo studies. Journal of biomedical materials research 2006;78(2):343–351. [PubMed: 16646066]
33. Hoban LD, Pierce M, Quance J, Hayward I, McKee A, Gowda DC, et al. Use of polypentapeptides of elastin to prevent postoperative adhesions: Efficacy in a contaminated peritoneal model. J Surg Res 1994;56(2):179–183. [PubMed: 8121175]
34. Wei SM, Katona E, Fachet J, Fulop T Jr, Robert L, Jacob MP. Epitope specificity of monoclonal and polyclonal antibodies to human elastin. Int Arch Allergy Immunol 1998;115(1):33–41. [PubMed: 9430493]
35. Meyer DE, Kong GA, Dewhirst MW, Zalutsky MRAC. Targeting a genetically engineered elastin-like polypeptide to solid tumors by local hypothermia. Cancer Res 2001;61:1548–1554. [PubMed: 11245464]
36. Liu W, Dreher MR, Chow DC, Zalutsky MR, Chilkoti A. Tracking the in vivo fate of recombinant polypeptides by isotopic labeling. J Control Release 2006;114:184–192. [PubMed: 16904221]
37. Betre H, Liu W, Zalutsky MR, Chilkoti A, Kraus VB, Setton LA. A thermally responsive biopolymer for intra-articular drug delivery. J Control Release 2006;115(2):175–182. [PubMed: 16959360]
38. Mithieux SM, Rasko JEJ, Weiss AS. Synthetic elastin hydrogels derived from massive elastic assemblies of self-organized human protein monomers. Biomaterials 2004;25:4921–4927. [PubMed: 15109852]
39. Cappello J, Crissman JW, Crissman M, Ferrari FA, Textor G, Wallis O, et al. In-situ self-assembling protein polymer gel systems for administration, delivery, and release of drugs. J Control Release 1998;53(1–3):105–117. [PubMed: 9741918]
40. Hatefi A, Cappello J, Ghandehari H. Adenoviral gene delivery to solid tumors by recombinant silk-elastinlike protein polymers. Pharm Res 2007;24(4):773–779. [PubMed: 17308969]
41. Andersson M, Suska F, Johansson A, Berglin M, Emanuelsson L, Elwing H, et al. Effect of molecular mobility of polymeric implants on soft tissue reactions: An in vivo study in rats. Journal of biomedical materials research 2008;84(3):652–660. [PubMed: 17635028]
42. Butler K, Benghuzzui H, Tucci M, Cason Z. A comparsion of fibrous tissue formation surrounding intraperitoneal and subcutaneous implantation of ALCAP, HA, and TCP ceramic devices. Biomed Sci Instrum 1997;34:18–23. [PubMed: 9603006]
43. Shin H, Quinten Ruhe P, Mikos AG, Jansen JA. In vivo bone and soft tissue response to injectable, biodegradable oligo(poly(ethylene glycol) fumarate) hydrogels. Biomaterials 2003;24(19):3201–3211. [PubMed: 12763447]

44. Giavaresi G, Torricelli P, Fornasari PM, Giardino R, Barbucci R, Leone G. Blood vessel formation after soft-tissue implantation of hyaluronan-based hydrogel supplemented with copper ions. Biomaterials 2005;26(16):3001–3008. [PubMed: 15603795]
45. Puolakkainen P, Bradshaw AD, Kyriakides TR, Reed M, Brekken R, Wight T, et al. Compromised production of extracellular matrix in mice lacking secreted protein, acidic and rich in cysteine (SPARC) leads to a reduced foreign body reaction to implanted biomaterials. The American journal of pathology 2003 Feb;162(2):627–635. [PubMed: 12547720]
46. Barbosa JN, Madureira P, Barbosa MA, Aguas AP. The influence of functional groups of self-assembled monolayers on fibrous capsule formation and cell recruitment. Journal of biomedical materials research 2006;76(4):737–743. [PubMed: 16331651]
47. Nair A, Zou L, Bhattacharyya D, Timmons RB, Tang L. Species and density of implant surface chemistry affect the extent of foreign body reactions. Langmuir 2008;24(5):2015–2024. [PubMed: 18189430]
48. Voskerician G, Gingras PH, Anderson JM. Macroporous condensed poly(tetrafluoroethylene). I. In vivo inflammatory response and healing characteristics. Journal of biomedical materials research 2006;76(2):234–242. [PubMed: 16116600]
49. Meena R, Prasad K, Siddhanta AK. Effect of genipin, a naturally occurring crosslinker on the properties of kappa-carrageenan. Int J Biol Macromol 2007;41(1):94–101. [PubMed: 17339049]
50. Jeong B, Kibbey MR, Birnbaum JC, Won YY, Gutowska A. Thermogelling biodegradable polymers with hydrophilic backbones: PEG-g-PLGA. Macromolecules 2000;33:8317–8322.
51. Wilson JT, Cui W, Sun XL, Tucker-Burden C, Weber CJ, Chaikof EL. In vivo biocompatibility and stability of a substrate-supported polymerizable membrane-mimetic film. Biomaterials 2007;28(4): 609–617. [PubMed: 17055571]
52. van Wachem PB, van Luyn MJ, Olde Damink LH, Dijkstra PJ, Feijen J, Nieuwenhuis P. Biocompatibility and tissue regenerating capacity of crosslinked dermal sheep collagen. J Biomed Mater Res 1994;28(3):353–363. [PubMed: 8077250]
53. Zeeman R, Dijkstra PJ, van Wachem PB, van Luyn MJ, Hendriks M, Cahalan PT, et al. Crosslinking and modification of dermal sheep collagen using 1, 4-butanediol diglycidyl ether. J Biomed Mater Res 1999;46(3):424–433. [PubMed: 10398001]
54. Weadock KS, Miller EJ, Keuffel EL, Dunn MG. Effect of physical crosslinking methods on collagen-fiber durability in proteolytic solutions. J Biomed Mater Res 1996;32(2):221–226. [PubMed: 8884499]
55. Han B, Jaurequi J, Tang BW, Nimni ME. Proanthocyanidin: A natural crosslinking reagent for stabilizing collagen matrices. Journal of biomedical materials research 2003 Apr 1;65(1):118–124. [PubMed: 12635161]
56. Greenwald D, Shumway S, Albear P, Gottlieb L. Mechanical comparison of 10 suture materials before and after in vivo incubation. J Surg Res 1994;56(4):372–377. [PubMed: 8152233]
57. Altman GH, Diaz F, Jakuba C, Calabro T, Horan RL, Chen J, et al. Silk-based biomaterials. Biomaterials 2003 Feb;24(3):401–416. [PubMed: 12423595]
58. Rehakova M, Bakos D, Vizarova K, Soldan M, Jurickova M. Properties of collagen and hyaluronic acid composite materials and their modification by chemical crosslinking. J Biomed Mater Res 1996;30(3):369–372. [PubMed: 8698700]
59. Lee DH, Ko RK, Cho ZH, Kim SS. Applications of NMR imaging to the time-dependent swelling effect in polymers. Biomed Mater Eng 1996;6(5):313–322. [PubMed: 8986352]
60. Stabler CL, Long RC Jr, Constantinidis I, Sambanis A. In vivo noninvasive monitoring of a tissue engineered construct using 1H NMR spectroscopy. Cell Transplant 2005;14(2–3):139–149. [PubMed: 15881423]

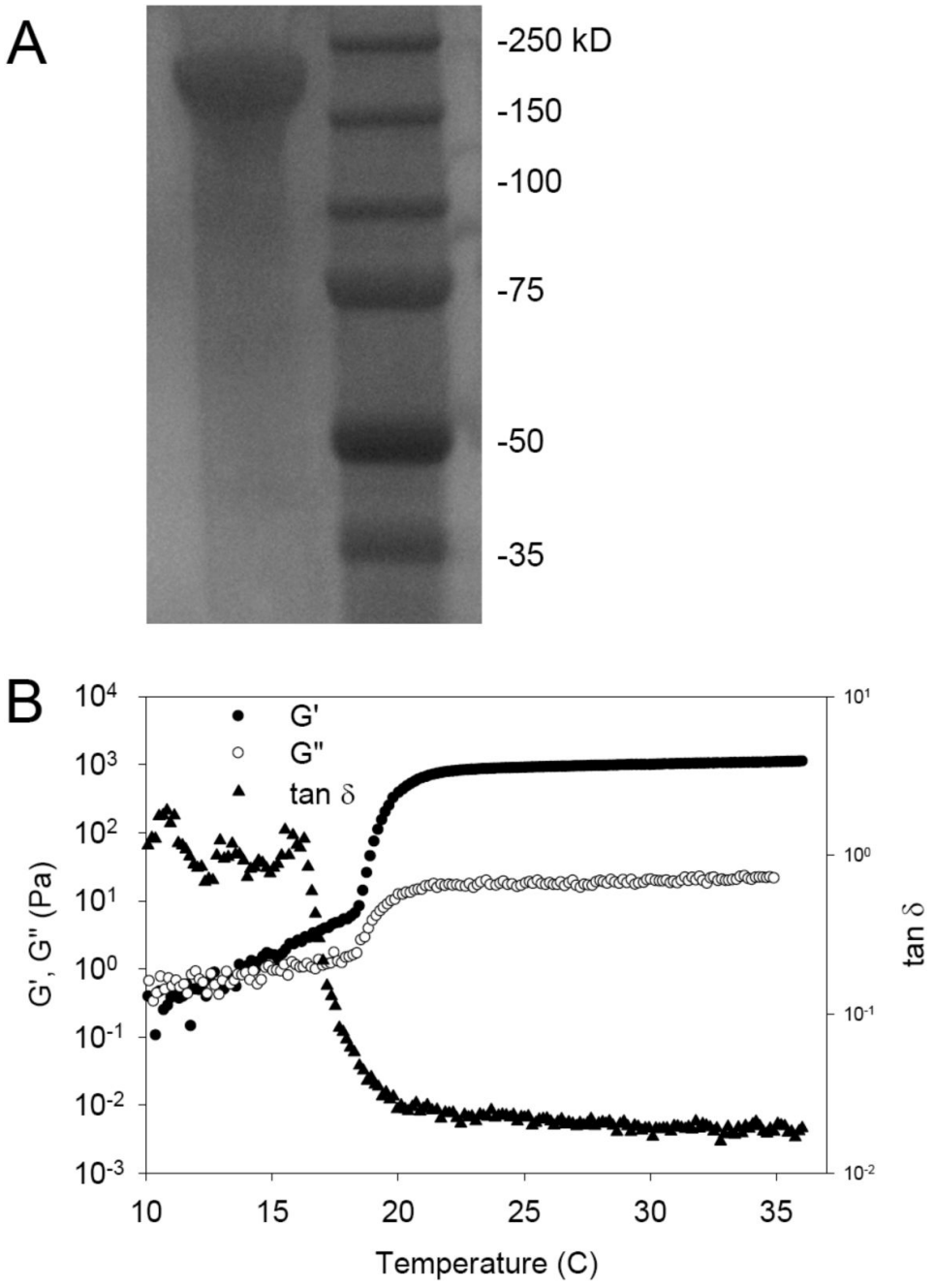

Figure 1. Structural characterization of a triblock elastin-mimetic protein polymer

(**A**) Sodium dodecyl sulfate-polyacrylamide gel electrophoresis (SDS-PAGE) analysis revealed a single protein band at 170 KDa corresponding to **B9**. A total of 10 μg of the elastin-mimetic polypeptide was run on 7.5% gel and negatively stained with Copper stain (Bio-Rad). Molecular weight markers were Precision Plus Protein Kaleidoscope (Bio-Rad). (**B)** Rheological behavior of 10-wt % **B9** in water. Dynamic shear storage (G′) and loss modulus (G″) are plotted as a function of temperature (γ2%, ω 1Hz). The gelation temperature was determined by heating samples from 4°C to 37°C at a rate of 1°C per minute. Experiments were repeated on three samples and representative data presented.

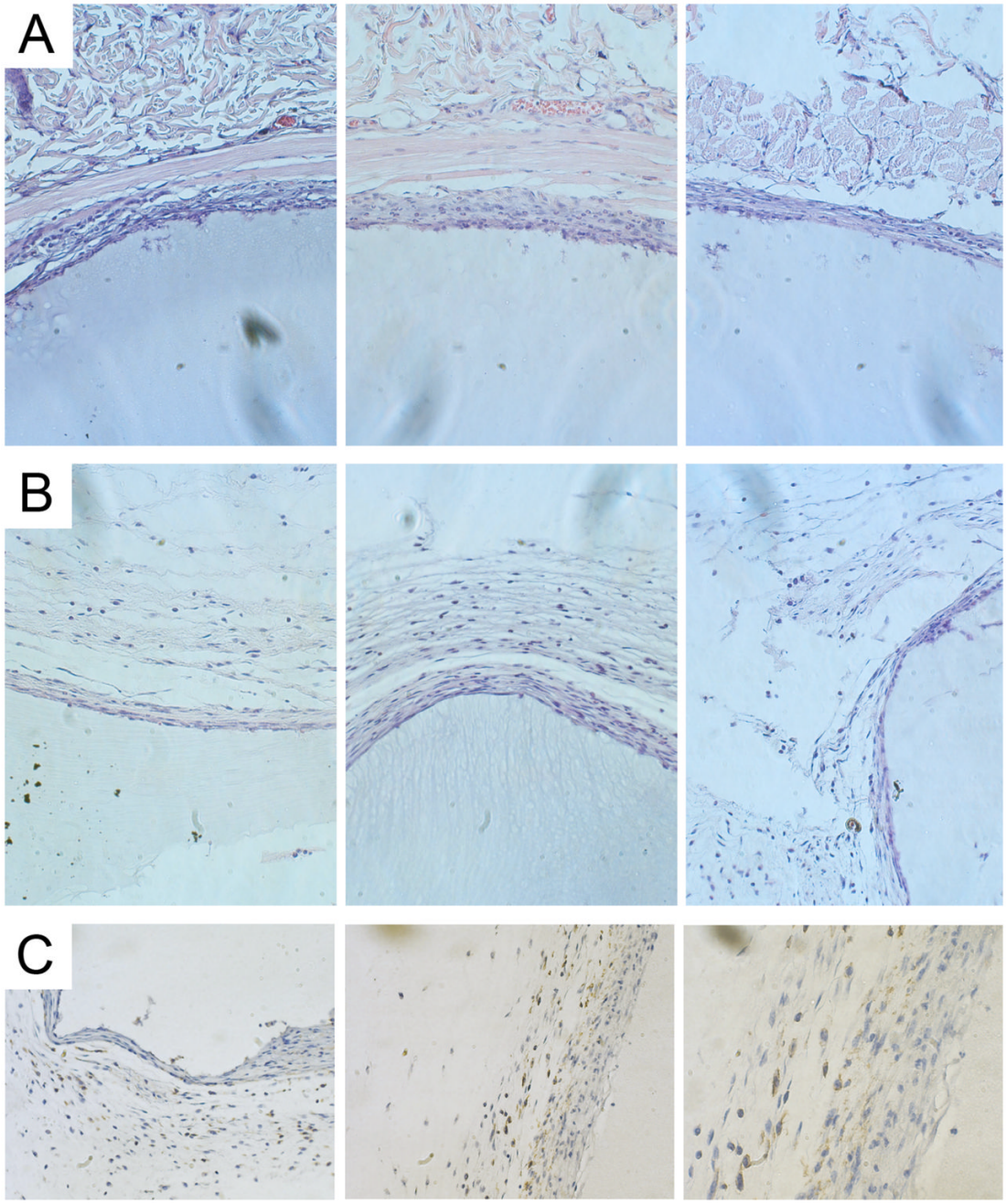

Figure 2. Short-term host-implant responses after subcutaneous injection of protein polymer in a mouse model

A 10 wt% solution of **B9** was injected subcutaneously, which gelled instantly. Samples were retrieved at 3 weeks and hematoxylin and eosin staining performed on formalin fixed, paraffin embedded implants. Histological analysis of the host response to the subcutaneous protein polymer implant was conducted at the implant-muscle **(A)** and implant-dermal **(B)** tissue interfaces. **(C)** F4/80 staining demonstrates the presence of macrophages along the periphery of the fibrous capsule but no infiltration into the implant. All images were obtained at 20x magnification.

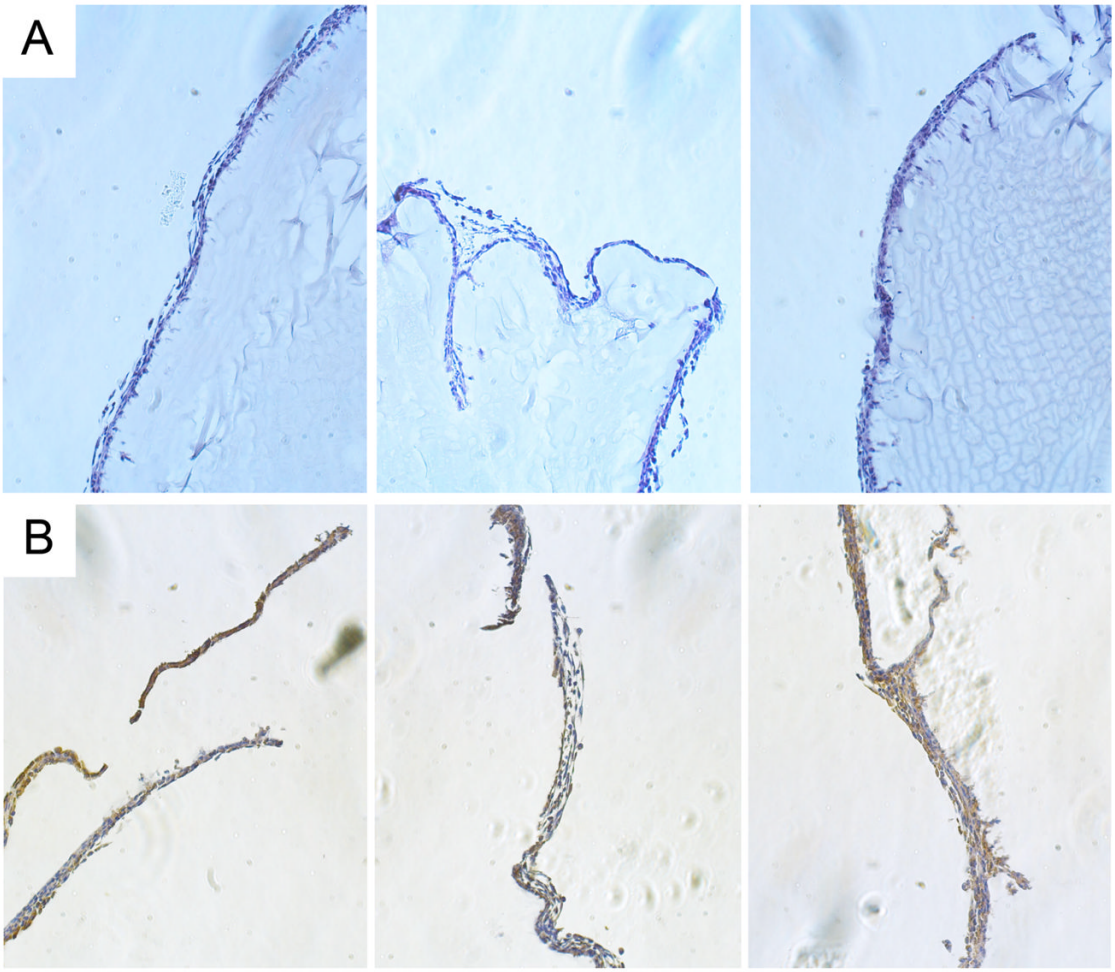

Figure 3. Short-term host-implant responses after peritoneal injection of protein polymer in a mouse model

(A) Histological analysis of hematoxylin and eosin stained formalin fixed, paraffin embedded peritoneal implants retrieved 1 week after implantation. **(B)** F4/80 staining of implants demonstrates the presence of macrophages along the periphery of the implant. All images were obtained at 20x magnification.

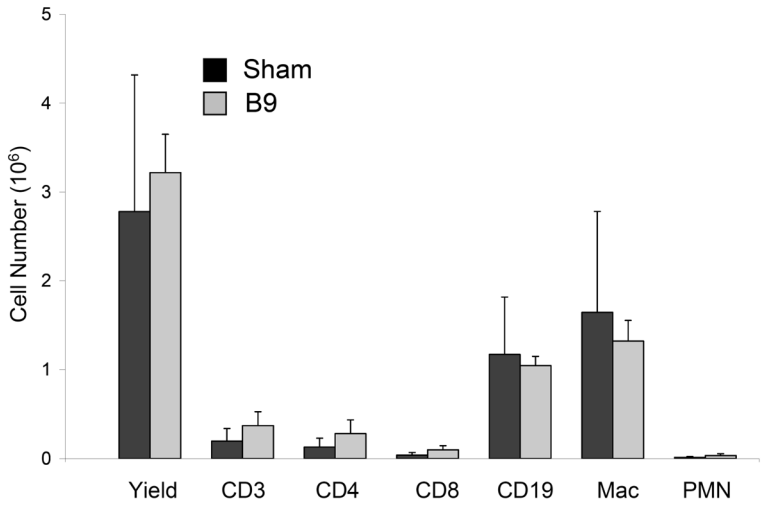

Figure 4. FACS analysis of peritoneal cell response to protein polymer implant 1 week after implantation

Cells from the peritoneal lavage were immunostained for flow cytometry with FITC-conjugated hamster anti-mouse CD3 for total T cells, FITC-conjugated rat monoclonal anti-mouse CD4 for helper T cells, FITC-conjugated rat monoclonal anti-mouse CD8 for cytotoxic T cells, FITC-conjugated rat monoclonal anti-mouse CD19 for B cells, PE-conjugated rat monoclonal anti-mouse CD11b for macrophage, and FITC-conjugated rat monoclonal anti-mouse Gr-1 for neutrophils. There was no observable difference in cellular response between mice receiving the implant or those that underwent sham surgery ($n=5$, $p < 0.05$).

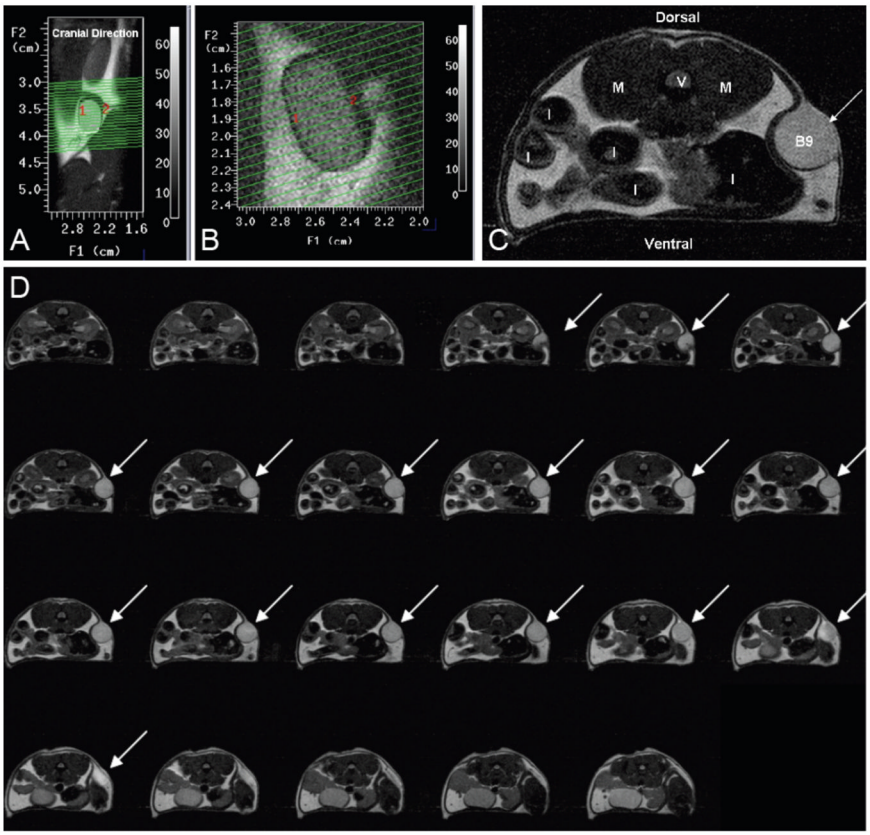

Figure 5. MR imaging of a subcutaneously implanted protein polymer cylindrical implant

(A) A coronal view through the mouse, oriented vertically, shows the location of the implant. The green lines depict 23 transverse-oblique slices through the implant. **(B)** MR scan slices through implant. **(C)** Transverse MR image of the subcutaneous **B9** implant. (V = verterbra, M = Psoas Major muscle, I = Intestine cross-sections, **B9** = cross-section of **B9** implant). **(D)** Sequential series of transverse MR images through a subcutaneously placed **B9** implant. Implant areas were assessed from individual images and summed to assess volume of the implant. Slice thickness is 500 μm.

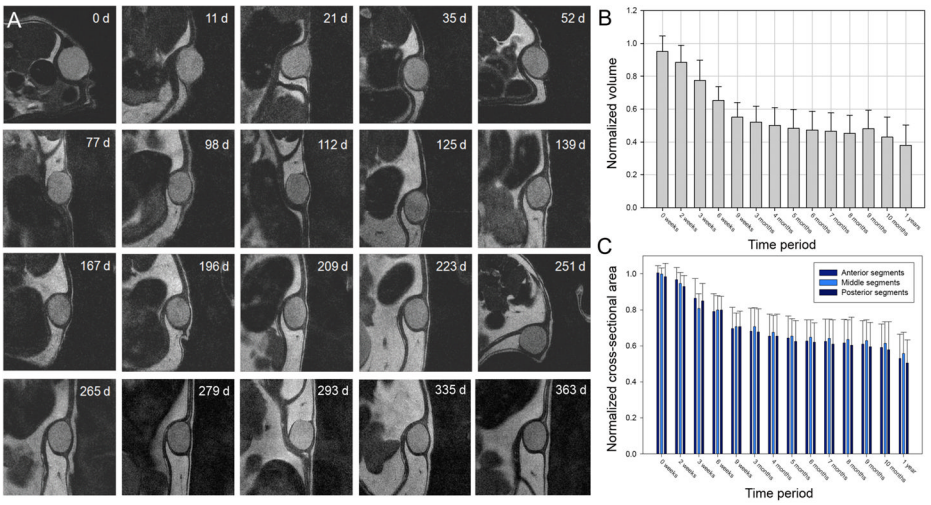

Figure 6. Serial MR imaging of subcutaneous protein polymer implants over a 12 month period

(A) Representative serial images of B9 implants over a 1-year period. Normalized implant volumes **(B)** and implant cross-sectional areas **(C)** were determined over a 1-year implant period (n = 7, mean ± SD).

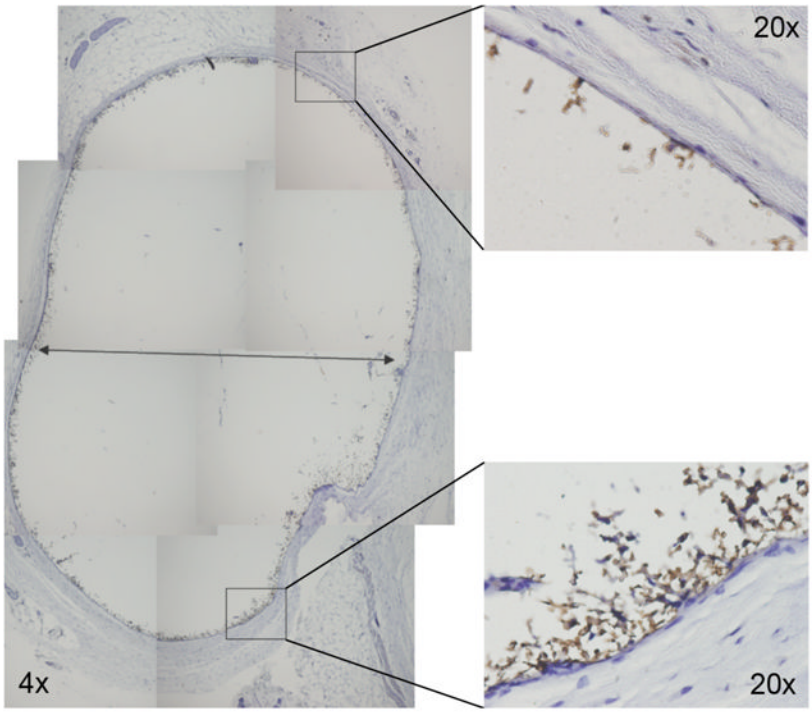

Figure 7. Histological analysis of protein polymer implants retrieved 1 year after implantation

F4/80 staining of formalin fixed, paraffin embedded **B9** implants demonstrate the presence of macrophages along the periphery of the fibrous capsule but no infiltration into the **B9** implant. Whole implant image was obtained at 4x magnification, while high power views were obtained at 20x magnification.

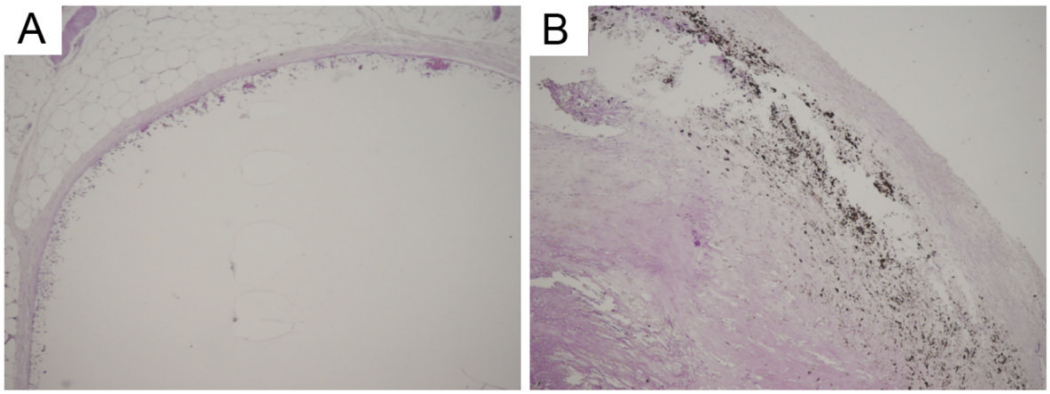

Figure 8. Histological analysis of protein polymer implants retrieved 1 year after implantation

Von Kossa staining does not reveal the presence of calcium in the **B9** implant (left), but demonstrates calcium deposits in a human carotid atherosclerotic plaque (right), used as a positive control. Images were obtained at 4x magnification.

-

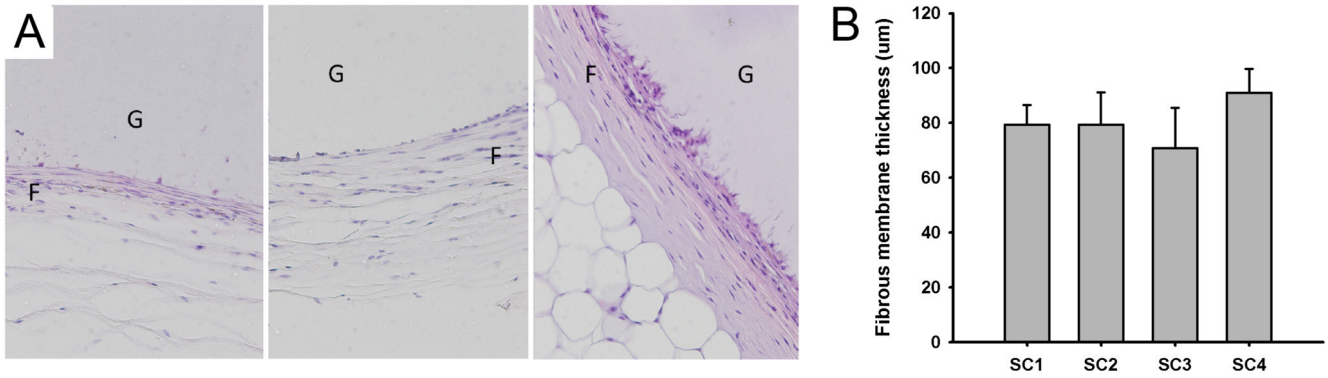

Figure 9. Analysis of fibrous capsule response to implants retrieved 1 year after implantation

(A) Histological examination of protein polymer B9 implanted in the dorsal subcutaneous space of C57BL/6 mice for 1 year. A fibrous capsule **(F)** was noted surrounding the protein polymer **(G)**. Samples were retrieved with capsule intact and hematoxylin and eosin staining performed on formalin fixed, paraffin embedded implants. **(B)** Capsule thickness was determined from measurements obtained from images obtained at 20x magnification from at least six distinct regions on each surrounding capsule in which each region is represented by a minimum of 10 high power fields. The capsule thickness is presented for four separate implants designated SC1 through SC4. The overall mean thickness ± standard deviation for all samples was 80 ± 8 μm.

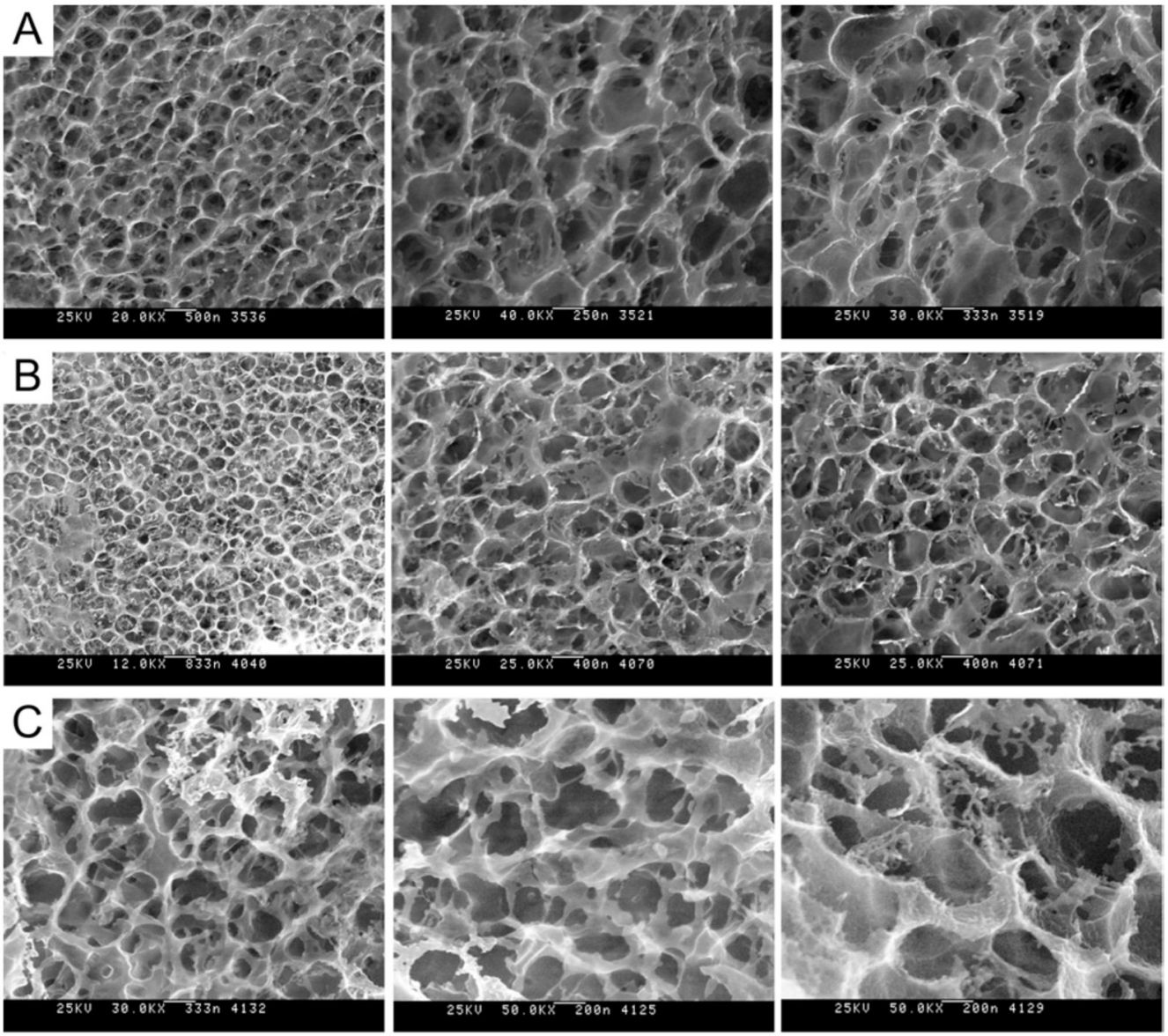

Figure 10. Cryo-HRSEM micrographs of protein polymer implants

(**A**) Images of hydrated 10-wt% B9 implants prior to implantation. After a 1-year implant period, implants were retrieved and the capsule removed. Cryo-HRSEM was performed to visualized the internal structure **(B)** of the implant after fracturing specimens with a pre-chilled blade and of the surface **(C)** of the implants. Magnification ranges from 25,000 to 50,000x.

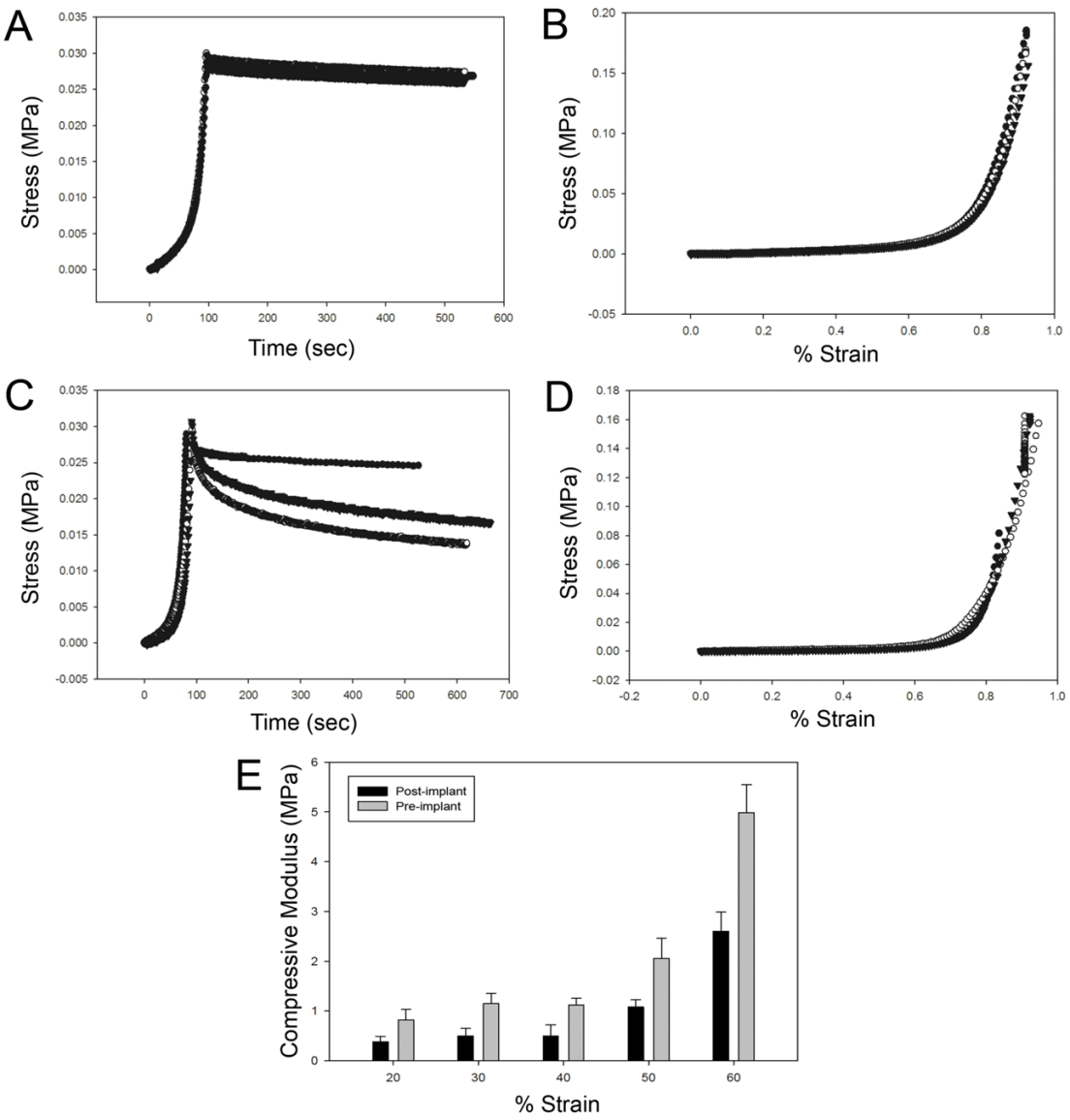

Figure 11. Biomechanical analysis of compression stress-strain responses of implants retrieved 1 year after implantation

Mechanical responses of protein polymer samples were characterized by compression testing prior to implantation (**A, B**) and at the time of specimen removal, one year after initial implantation (**C, D, E**). Cylindrical specimens were fabricated and cut to a thickness of 2.35 mm for mechanical testing in a Bose ELF system in a hydration chamber containing PBS at 37°C. Samples were preconditioned by cyclic compression ranging between 1% and 20% strain for 10 cycles. Compression stress-relaxation testing was conducted by compressing the sample to a strain of 75% at 0.025 mm/sec followed by monitoring change in compression stress over time (**A, C**). Compression stress-strain testing was performed at 0.025 mm/sec (**B, D**). Cotangent moduli (**E**) were calculated from the compression stress-strain plots at 10% strain intervals between 20% and 60% strain.

Table 1

Biocompatibility of Chemically Synthesized and Recombinant Elastin-Mimetic Polypeptides

Recombinant Elastin-Mimetic	Assay	Reported Results	Testing Comments
Chemically synthesized Poly (VPGVG)	Ames mutagenicity test	Non- mutagenic	Test samples were determined as innocuous as negative controls 55
Chemically synthesized Poly (VPGVG)	Cytotoxicity-agarose overlay	Non-toxic	No evidence of fibroblast cell death or lysis following incubation for 24 hours 55
Chemically synthesized Poly (VPGVG)	Acute systemic toxicity	Non-toxic	No difference in IV injections of 24 hour extracts of gamma irradiated sheets of poly(VPGVG) and control extracts 55
Chemically synthesized Poly (VPGVG)	Intracutaneous toxicity	Non-toxic	No erythema or edema was observed at injection site after 24, 48, and 72 hours 55
Chemically synthesized Poly (VPGVG)	Muscle implantation	Favorable at 7 days	Needle injection of film fragments, material was a ‘slight irritant’ as compared to the negative control 55
Chemically synthesized Poly (VPGVG)	Acute intraperitoneal toxicity	Non-toxic at 4 weeks	Recovered implants were reported as ‘very similar to pre-implant condition’ 55
Chemically synthesized Poly (VPGVG)	Systemic antigenicity study	Non-antigenic	No anaphylactic signs from IP injections three times a week, every other day, for 14 and 21 days 55
Chemically synthesized Poly (VPGVG)	Dermal sensitation	Non- sensitizing at 7 days	Intradermal injections were challenged with solutions to provoke a mild acute inflammation at injection site, but ‘showed no significant evidence of causing dermal sensitization 55
Chemically synthesized Poly (VPGVG)	Pyrogenicity	Non-pyrogenic	IV injection into rabbit ear vein and temperature of the animals were monitored 55
Chemically synthesized Poly (VPGVG)	Lee White Clotting Study	Normal clotting time	Used canine blood, all clotting times were within normal ranges for dog 55
Chemically synthesized Poly (VPGVG)	*In vitro* hemolysis test	Non-hemolytic	0% hemolysis reported for rabbit blood determined spectrophotometrically 55
Chemically synthesized Poly (VPGVG)	Bone implantation	No calcification or ossification	Fibrous granulation tissue, no calcification or ossification at 3 weeks 54
Chemically synthesized Poly (VPGVG)	IM implantation	No calcification or ossification	Fibrous tissue capsule with a medium range of active phagocytic cell infiltration at muscle site with no evidence of calcification or ossification, reported as ‘passive tissue reaction similar to those found for biodegradable suture materials at three weeks 54
Microbially expressed triblock	Baboon arteriovenous shunt model	Non-thrombogenic	Minimal fibrin and platelet deposition over a 1 hour time period of elastin-mimetic impregnated PTFE graft 19
Chemically synthesized Poly (VPAVG)	Subcutaneous injection	Non-inflammatory	Edema was measured after microparticle injection at 24 hours in a hind paw injection model 56
Chemically synthesized Poly (VPAVG)	Intraocular injection	Non-inflammatory	28 days post-injection displayed minimal signs of inflammation, though tractional retinal detachment was observed with fibroblastic activity 56
Microbially expressed poly VPGVG (aggregating) and VPGAG (non-aggregating)	Intra-articular injection	Biodegradable	Protein remained in joint for 2 (non-aggregated protein) to 30 days (aggregated protein) [61]
Microbially expressed human tropoelastin	Subcutaneous implant	Well tolerated	Uniform encapsulation with minimal to moderate inflammation at 13 weeks [62]